

Investigation of the Dynamic Plate Loading Test with the Light-Weight Deflectometer using the Boundary Element Method

Dipl.-Ing. Dr.techn. Fritz KOPF

Univ.Doiz. Dipl.-Ing. Dr.techn. Dietmar ADAM

Dipl.-Ing. Ivan PAULMICHL

ABSTRACT

The dynamic plate loading test using the Light-Weight Deflectometer is an innovative field test designed to determine the dynamic deformation modulus of subsoils and fills in all types of earth working and ground engineering applications. In earth working, the test can be used for compaction control and for assessing the load-bearing capacity of the subsoil.

This article compares the results of numerical investigations on the Light-Weight Deflectometer obtained with the boundary element method against results from experimental tests.

1. INTRODUCTION

The dynamic plate loading test using the Light-Weight Deflectometer (LWD) has been developed as a test procedure for the determination of the dynamic deformation modulus E_{vd} of soils and unbound fill materials [12], [9].

The test consists of subjecting the soil to a pulse load applied via a disk-shaped steel plate that is assumed to be rigid. The loading mechanism consists of a drop weight that, once released, falls along a rod until it hits a dashpot unit. The loading device is positioned on a centring sphere in the middle of the disk so that only compressive forces can be transmitted to the loading plate. A sensor connected to an electronic meter is installed in the middle of the plate. It records the movements of the plate even while the test is being carried out (see Fig. 1) [1].

The evaluation procedure is based on a simple principle. After completion of the test, the maximum displacement of the plate is calculated by means of double/single integrals of the accelerations and oscillation speeds. All other parameters required for determining the dynamic deformation modulus, including specifically contact stress between the plate and the ground, are assumed to be constant. This approximation, which has been recognised as appropriate, can be justified by the mutual adjustment of equipment parameters and their

adjustment to the subsoil characteristics being expected. These adjustments and the resulting equipment configuration are based on extensive model calculations and parameter studies conducted primarily by *Weingart* and published as early as 1977 as part of his dissertation [12], [13].

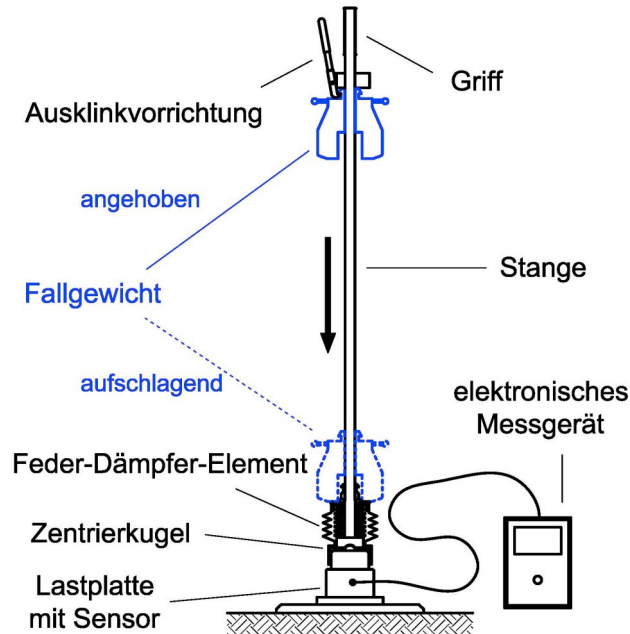


Fig. 1: Components of the Light-Weight Deflectometer [1], [5].

2. TEST SPECIFICATION FOR LIGHT-WEIGHT DEFLECTOMETER

2.1. General requirements and equipment calibration

The relevant equipment parameters have been standardised to create uniform boundary conditions for conducting tests with different LWD products. Detailed instructions are provided in the German specification TP BF StB, Part B 8.3 edition 2003 “Dynamischer Plattendruckversuch mit Leichtem Fallgewichtsgerät” [10] (dynamic plate loading test using the Light-Weight Deflectometer) issued by Forschungsgesellschaft für Straßen- und Verkehrswesen. The specifications given in Table 1 thus have to be complied with within the tolerances specified.

An important part of the Test Specifications is the instructions for the calibration of the LWD, which has to be carried out by recognised institutions prior to delivery, after repair work and periodically at least once a year.

The loading device (peak value of load pulse) is calibrated by adjusting the drop height of the device. In devices using (steel) disk springs, changing the stiffness of the spring can be used additionally for calibration purposes.

The deflectometer has to be adjusted to the measuring range of the deflection amplitude indicated in Table 1 by means of the previously calibrated drop weight. Beyond that, the user has to check the deflectometer periodically by means of a simplified procedure.

Table 1: Requirements to be met by the Light-Weight Deflectometer according to TP BF StB, Part B 8.3.

| | | |
|---|------------------------------------|--|
| <u>Load plate</u> made of steel, minimum St 52-3 (tolerance for equipment dimensions: 1%) | | |
| Diameter | 300 mm | ± 0.5 mm |
| Plate thickness | 20 mm | ± 0.2 mm |
| Mass 15 kg | ± 0.25 kg (incl. sensors, handles) | |
| Roughness | max. 6.3 µm | |
| <u>Deflectometer</u> | | |
| Frequency range | 8 – 100 Hz | (temperature 0 to 40°C) |
| Deflection amplitude | 0.3 – 1.5 mm | Minimum measuring accuracy ± 0.015 mm (simplified) |
| <u>Loading mechanism</u> | | |
| Mass of drop weight | 10 kg | ± 0.1 kg |
| Total mass of guide rod | 5 kg | ± 0.1 kg (incl. dashpot unit) |
| Maximum pulse load | 7.07 kN | (± 1%, temperature 0 to 40°C) |
| Duration of load pulse | 17 ms | ± 1.5 ms |

The equipment dimensions and masses listed in the Table above were used for the numerical investigations with the boundary element method.

2.2. Standardised test procedure and analysis

In the standardised test procedure, the plate is placed to rest horizontally and firmly on the site to be tested. A thin layer of sand may have to be placed below the plate to compensate for any unevenness. Three seating drops should be made to produce full contact between the plate and the soil. Then three further drops are made in the same manner, for which the plate displacement is recorded by means of the electronic meter. The mean value of the three peaks of vertical displacements recorded (designated “Setzung *s*” (“deflection *s*”) in the specification) forms the basis for the determination of the dynamic deformation modulus E_{vd} . For this purpose, two simplifying assumptions are made:

The dynamic plate loading test is evaluated using the formula of the static plate load test, which is based on the theory of the statically loaded elastic halfspace:

$$E_v = 1,5 \cdot r \cdot \frac{\Delta\sigma}{\Delta z} \quad (1)$$

with E_v being the deformation modulus of the subsoil, r the radius of the plate, $\Delta\sigma$ the change in mean contact pressure, and Δz the corresponding vertical displacement of the plate. This

simplified approach ignores, however, speed-related factors and inertial forces in the evaluation of the test.

In addition, it is assumed hypothetically that the maximum mean load σ acting on the soil during the test is generally a constant (0.1 MN/m²). This simplification degenerates equation (1) for a load plate with a diameter of 30 cm to the following term for the dynamic deformation modulus:

$$E_{vd}[\text{MN/m}^2] = \frac{22,5}{z_{max}[\text{mm}]} \quad (2)$$

Thus, determination of E_{vd} in the analysis of the LWD test is based solely on the peak deflection z_{max} recorded (Fig. 2) [3].

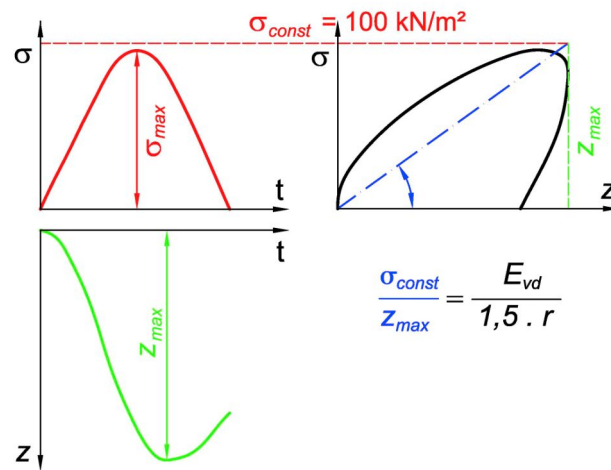


Fig. 2: Load acting on the soil and displacement and working diagram of the LWD plate [1], [5].

3. NUMERICAL ANALYSES OF THE DYNAMIC PLATE LOADING TEST USING THE BOUNDARY ELEMENT METHOD

3.1. The boundary element method and its application in numerical analyses with the substructure method

The basic principle underlying the boundary element method (BEM) is that the variables "path" and "force" recorded on the boundary of a component uniquely define the strains and stresses in its interior [4], [8]. Hence, the influence functions and coupling conditions are related only to the boundary of the area being investigated. The dimension of the problem being considered is thus reduced by one dimension. A 3-dimensional body therefore has to be discretised only on its 2-dimensional surface. 2-dimensional problems are reduced to consideration of the 1-dimensional boundary line. The number of degrees of freedom and thus

the dimension of the equation to be solved is thus reduced significantly compared with domain methods such as the finite elements methods (FEM). A crucial advantage, specifically in dynamic tests, is that BEM allows the formulation of boundary conditions even at infinity. Thus, at such a boundary defined by “semi-infinite” elements (“enclosing elements”), the energy of a compression or shear wave can dissipate into the simulated half-space without any significant reflections, allowing the so-called geometric damping of the half-space to be accounted for “with accuracy”. The FEM and other domain methods also allow the definition of “semi-infinite” elements, but their use is much more problematical than BEM in terms of theory and computational effort.

Once a model has been solved with BEM on the boundary of the area examined, all state variables at any point within the domain can be determined from this result in post-processing calculations. The BEM approach satisfies the differential equations fully. Discretisation is carried out only at the boundary, with the resulting errors decreasing with increasing distance from the discretised boundary in accordance with *Saint Venant's* principle. Such inexactness at the boundary is due to the fact that it is impossible to solve the integration analytically in closed form. Thus, the integration has to be carried out numerically, which, however, can be done much more exactly and in a more stable manner than a numerical differentiation. Compared with FEM, BEM produces a smaller system of equations and thus requires less computation time while yielding higher computational accuracy.

While BEM offers some advantages over domain methods, it also has a number of practical and theoretical limitations and drawbacks. Thus, the unique description of an area through discretisation requires the behaviour of the material on its boundary to be linear elastic. While there are theoretical approaches for expanding the application of BEM to non-linear material behaviour, the method loses much of its power in the process. In testing soil dynamics, the restriction to linear elastic problems is not a major drawback, however, and one may exploit the validity of the superposition law that is thus ensured. In contrast to FEM, BEM equations contain non-symmetrical matrices, which require a slightly more complex solution algorithm. Since with BEM, only the boundary has to be discretised, significantly smaller equation systems are obtained than with FE calculations in similar investigations, and their lack of symmetry is therefore not much of a problem.

At the time when BEM was developed FEM was already well-established in research and practice. So far, BEM has been unable to catch up with FEM and therefore the few BEM programs that are currently on the market are relatively poorly conceived and not very user friendly.

It is against this backdrop that the following choice of procedure must be seen, in which the BEM program used (GPBEST, BESTVIEW) allows dynamic problems to be dealt with in the time domain by not more than 20 time steps and in which it is not feasible to transfer the result obtained for use as an initial condition in subsequent calculations [2], [6]. This is unacceptable for all dynamic problems arising in practice. Therefore, a much more complex approach had to be chosen. The effort involved was justifiable in a university research setting but would have been inconceivable in practice.

3.2. Sub-structure method

The BEM programme used has the capability to analyse structures in the frequency domain. The solution of the LWD-soil dynamic interaction system including the drop weight contact problem (impact, rebound) is not possible in the frequency domain. For this reason, the system is split into two sub-structures. The two sub-systems are solved separately from each other and then, by satisfying the compatibility conditions (force and displacement), coupled again at the interface [7].

3.2.1. Sub-structure 1: Drop weight and dashpot unit

Sub-structure 1 comprises the part of the interaction system that has to be solved in the time domain. It consists of the drop weight and the dashpot unit plus the corresponding contact and rebound condition while the load plate with the rod and its masses are regarded as part of the second sub-structure. The interface between the two sub-systems is the place where the dashpot unit is connected to the load plate. At this interface, the compatibility conditions regarding force (or stress) and displacement must be satisfied when the systems are coupled together.

For the first sub-structure, a function $z(t)$ is assumed for the displacement of the bottom end of the dashpot unit. When the drop weight hits the dashpot unit, the load plate is still at rest and thus $z(0) = 0$ and $\dot{z}(0) = 0$, as the displacement (= deflection of the load plate) is caused only by the impact. The load plate displacement $z(t)$ affects the progress of the impact, which the drop weight transmits via the dashpot unit. The aim is to determine the force progression $F(t)$ of the pulse for any function of the plate displacement $z(t)$.

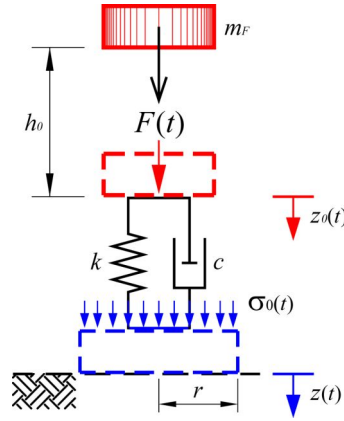


Fig. 3: Sub-structure 1: Drop weight and dashpot unit [7].

When an impact is simulated, the drop weight hits the dashpot unit initially at a velocity of \dot{z}_0 (Equation 3).

$$\dot{z}_0 = \sqrt{2 \cdot g \cdot h} \quad (3)$$

At this time the contact phase starts in which the dashpot unit transmits compressive forces from the drop weight to the load plate. The linear momentum equation for the drop weight can be formulated as follows:

$$m_F \cdot \ddot{z}_0 = m_F \cdot g - k \cdot (z_0 - z) - c \cdot (\dot{z}_0 - \dot{z}) \quad (4)$$

From this, the drop weight acceleration in the contact phase ($\ddot{z}_0 < g$) is derived:

$$\ddot{z}_0 = g - \frac{k \cdot (z_0 - z) + c \cdot (\dot{z}_0 - \dot{z})}{m_F} \quad (5)$$

Loading of the load plate with the radius r

$$F(t) = k \cdot (z_0 - z) + c \cdot (\dot{z}_0 - \dot{z}) = m_F \cdot (g - \ddot{z}_0) \quad (6)$$

produces a mean plate loading stress

$$\sigma_0(t) = \frac{F(t)}{A_{pl}} = \frac{m_F \cdot (g - \ddot{z}_0)}{r^2 \cdot \pi} \quad (7)$$

which acts in the place where the substructures are coupled. It can be computed through direct numerical integration of the differential equation.

At the end of the contact phase, the rebound condition ($\ddot{z}_0 = g$) commences. At this time, the drop weight floats and does not transmit any forces. In a permanently coupled system, this would be the time when the sign of the loading force changes. However, as the drop weight can exert compressive forces only on the dashpot unit, de-coupling occurs at this point and the drop weight rebounds, leaving the loading force at zero.

In order to determine the mean ground contact stress, stresses caused by inertial forces have to be deducted from the load-induced stress.

$$\sigma(t) = \frac{m_F \cdot (g - \ddot{z}_0) - (m_{Pl} + m_{St}) \cdot \ddot{z}}{r^2 \cdot \pi} \quad (8)$$

Table 2: Equipment parameters for numerical simulation.

| Equipment parameters | Symbol | Size | Unit |
|----------------------|----------|-----------|---------|
| Drop weight | m_F | 10 | kg |
| Drop height | h_0 | 70 | cm |
| Mass of load plate | m_{Pl} | 15 | kg |
| Mass of guiding rod | m_{St} | 5 | kg |
| Stiffness of spring | k | 337112,52 | N/m |
| Damping of spring | c | 129,9147 | N/(m/s) |

3.2.2. Sub-structure 2: Soil and plate

Substructure 2 includes everything that can be dealt with by BEM in the frequency domain (Fig. 4). This comprises the (layered) subsoil and the plate. The problem is defined by means of a plane rotationally symmetric model. The soil surface is loaded only by the plate. The remaining boundaries are modelled using semi-infinite elements simulating the half-space.

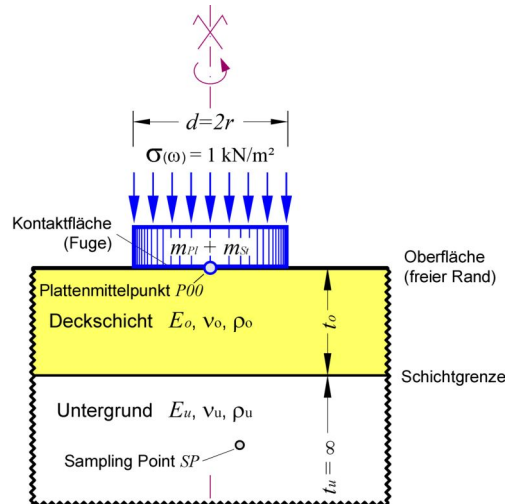


Fig. 4: Sub-structure 2: soil and plate [7].

The top side of the plate is loaded harmonically with a unit load of a 1 kN/m² at different frequencies (angular frequency $\omega=2\pi f$). The result of the BEM calculation is the system response in the defined boundary points and in selected domain points, with the latter being implemented in the model by means of elliptical co-ordinates (Fig. 5). Special attention is given to the result of the plate centre $P00$, as this is needed for coupling the substructures.

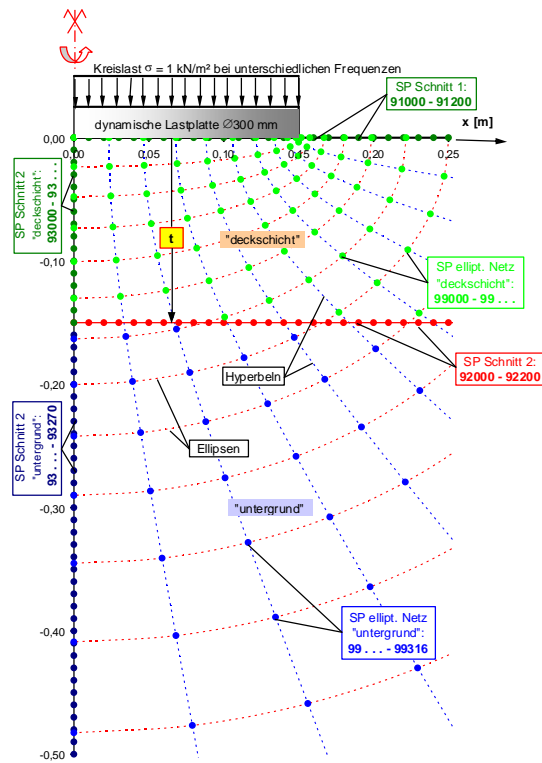


Fig. 5: Rotationally symmetric simulation model for the BEM simulation of the dynamic plate load test; section with boundary and domain points [7].

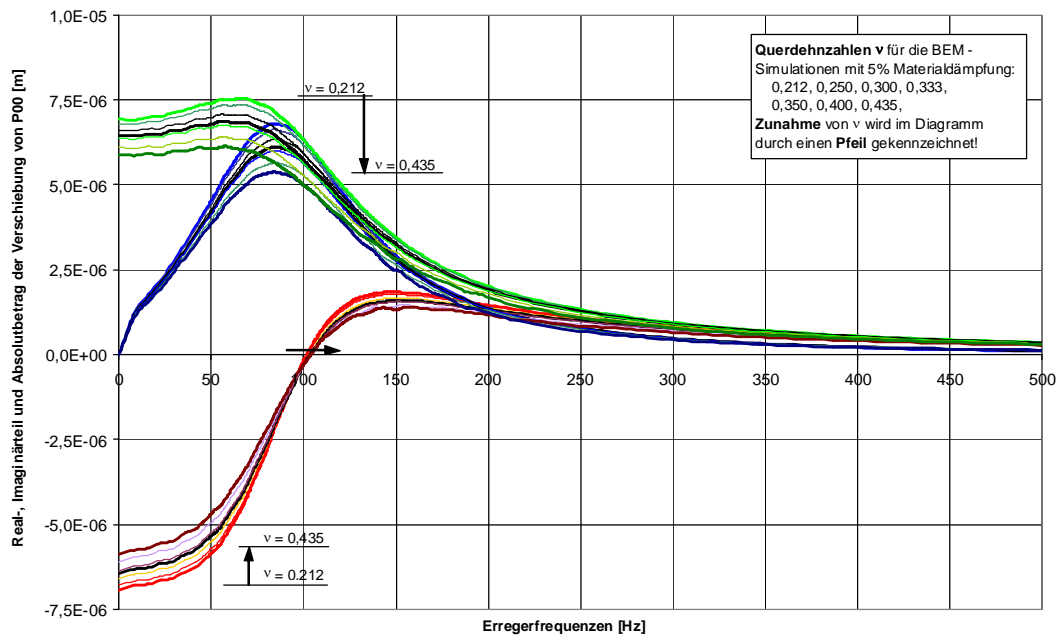


Fig. 6 Transmission functions for the plate centre $P00$ of a load plate ($r = 150\text{mm}$, $m = 20\text{kg}$, $\Delta\sigma = 1\text{kN/m}^2$) to a homogeneous half-space ($E_o = E_u = 32\text{ MN/m}^2$, $\rho_o = \rho_u = 2000\text{ kg/m}^3$) for various Poisson's ratios. BEM simulation at 5% material damping (hysteretic), [7]. Red: real portion; blue: imaginary portion; green: absolute amount.

Figure 6 shows the transmission functions $Z(\omega)$ of the displacements of the plate centre $P00$ determined by BEM in the frequency domain. For the Poisson's ratios ν investigated, the simulation model was calculated by means of BEM in the frequency domain from 0 Hz to 500 Hz. For each examined frequency ω , one imaginary number (real and imaginary portions: red and blue in the diagram) was obtained, which describes the phasing of the system response and, by the absolute amount (green in the diagram), the amplitude. Material damping was assumed to be relatively low at 5%. Given the geometric damping of the half-space, material damping would not even have been necessary at all but it provides for smoother transmission functions. With the BEM program used, damping can be taken into account only in the form of a complex stiffness matrix, which allows only hysteretic damping (with damping forces being proportional to the elastic forces) but no viscous damping (damping forces proportional to frequency). In the static case (excitation frequency = 0 Hz), the imaginary portion of the transmission function would have to disappear, which with viscous damping is actually the case. With hysteretic damping, the imaginary portion does not converge to zero as the excitation frequency falls, however, which may produce false results. At high frequencies, calculations with hysteretic damping often provide more realistic results than with viscous damping. In the parametric studies, material damping was ignored.

3.2.3. Coupling the substructures

The interaction system is now solved iteratively:

Substructure 1 is solved initially without plate displacement ($z(t) = 0$). The result $\sigma_0(t)$ is transformed into the frequency domain using Fourier transformation $\sigma_0(\omega)$. The solution for substructure 2 in the frequency domain is obtained by multiplying stress by the transmission function $Z(\omega)$.

$$z(\omega) = \sigma_0(\omega) \cdot Z(\omega) \quad (9)$$

The plate displacement $z(\omega)$ calculated in this manner in the frequency domain is then transformed into the time domain by inverse Fourier transformation and is used as new assumption for $z(t)$ in substructure 1.

This cycle is continued until convergence is achieved. Convergence means that $z(t)$ and $\sigma_0(t)$ (and the corresponding $z(\omega)$ and $\sigma_0(\omega)$) represent solutions for both substructures. Therefore, the compatibility conditions at the interface of the structures are satisfied and the structured are thus coupled.

It is only after coupling that the transmission functions $Z_{SP}(\omega)$ and $\Sigma_{SP}(\omega)$ are required for the domain points (“sampling points”) in order to obtain the state variables in the frequency domain through multiplication by the “final” load $\sigma_0(\omega)$. These are transformed into the time domain through inverse Fourier transformation.

$$z_{SP}(\omega) = \sigma_0(\omega) \cdot Z_{SP}(\omega) \rightarrow \text{inverse FFT} \rightarrow z_{SP}(t) \quad \text{Displacements over time} \quad (10a)$$

$$\sigma_{SP}(\omega) = \sigma_0(\omega) \cdot \Sigma_{SP}(\omega) \rightarrow \text{inverse FFT} \rightarrow \sigma_{SP}(t) \quad \text{Stresses over time} \quad (10b)$$

Now the data are available for further processing. A program for the individual time steps assigns them to the corresponding points by colour. The resulting images are combined into a video that illustrates the change in the individual state variables during an impact (Table 4).

Figure 7 illustrates the procedure described and Table 3 lists the programs required. This demonstrates the level of effort needed, which can be undertaken within the framework of a scientific study of a soil dynamics problem but which appears disproportionately large for the standardised management of problems arising in the field in practice.

Table 3: Programs required for the numerical simulation of the dynamic load plate using the boundary element method [7].

| No. | Program | Task |
|-----|----------------------|---|
| 1 | FORCE | Writing FORTRAN programs |
| 2 | EXCEED | Link to work station |
| 3 | BESTVIEW | Modelling of substructure 2, generation for GPBEST |
| 4 | vi-Editor | Modification of generated BESTVIEW file |
| 5 | FORTRAN | Generating files with sampling points and the file with the excitation frequencies |
| 6 | batch job under UNIX | Modification of edited BESTVIEW file, starting BEM calculations and production of result files |
| 7 | GPBEST | BEM calculation (for calling by batch job see No. 6) |
| 8 | FORTRAN | Reading transmission functions for the place centre and sampling points. |
| 9 | FTP | File transfer (UNIX-WINDOWS) |
| 10 | MATLAB | Reading transmission function for the plate centre. Solution for substructure 1 and iterative coupling of the two substructures (in frequency and time domains) |
| 11 | MATLAB | Reading the transmission functions of all sampling points. Computing sampling points using the solution obtained (No. 10) and the transmission functions in the frequency domain, transformation in the time domain, generation of colour images (stresses, velocity, deformation...) |
| 12 | EXCEL | Presentation of characteristics of dynamic load plate tests on homogenous and layered half-spaces |
| 13 | PREMIERE | Combination of colour images into a video |

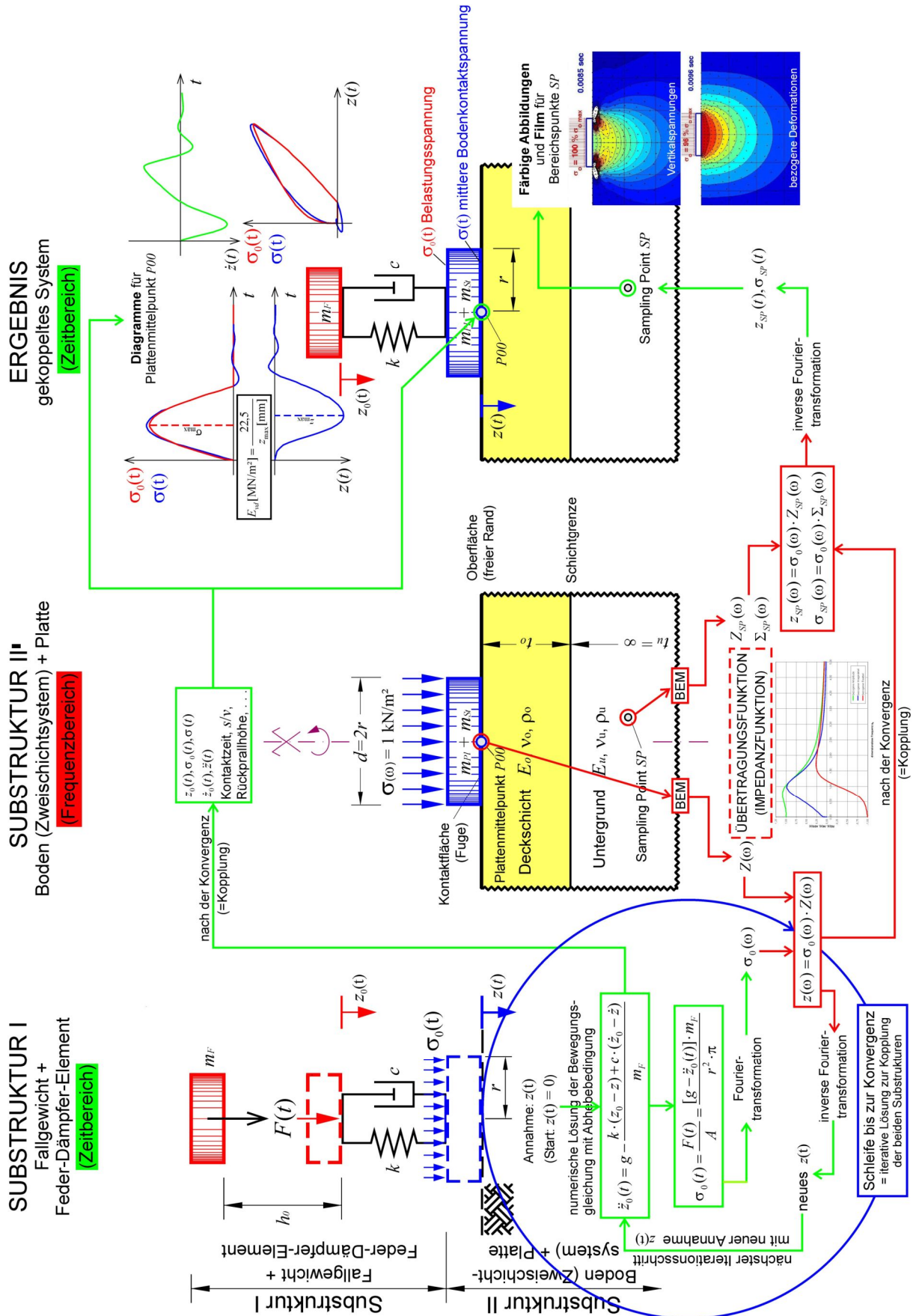


Fig. 7: Illustration of substructure method and the solution path for coupling the structures for simulating the dynamic load plate using BEM [7].

Figure 8 shows a typical result after coupling of the structures. The top left chart shows the stress caused by the impact of the drop weight (red) and the soil contact stress taking into account the inertial forces of the plate and of the rod (light blue). One can see that with this calculation brief tensile stresses occur in the plate-soil contact joint after the impact. In practice, however, this will happen only in the case of cohesive soils and will not exceed the magnitude of the air pressure. However, as in all evaluations of the dynamic load plate test only the loading phase is of relevance, this effect can be ignored. The top right diagram shows the development of velocity. The green line in the bottom left chart shows the soil displacement, the bottom right working diagram plots the stress caused by the impact of the drop weight (magenta-coloured points) and soil contact stresses (blue line). The dynamic nature of the test is reflected by the fact that maximum displacement occurs only after the time of maximum loading.

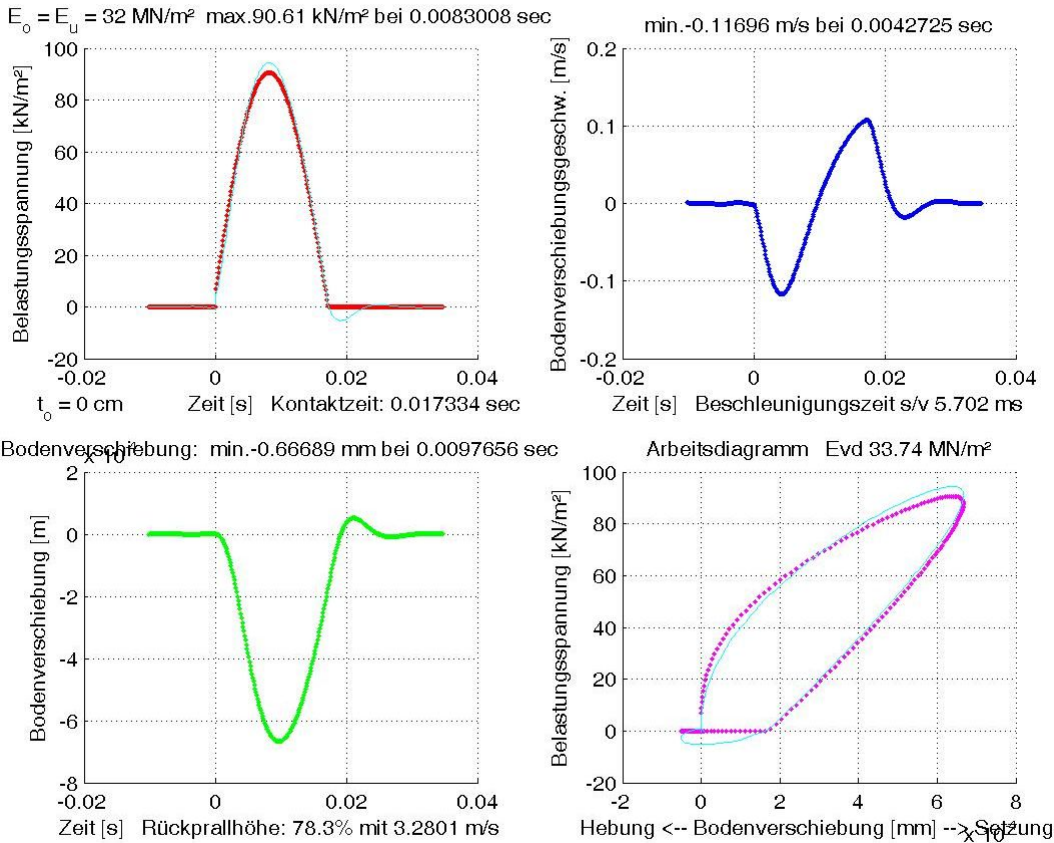


Fig. 8: MATLAB result sheet for a coupled system (homogenous half-space, $E = 32 \text{ MN/m}^2$, without material damping) with the transmission function derived from the BEM computation [7].

Table 4 shows the time sequence (from the start of the contact phase) of the related vertical displacements (in % of maximum displacement), which is the result of the computation of a

dynamic plate loading test on a layered subsoil after coupling of the substructures. A layer of 30 cm thickness with a modulus of elasticity of $E_o = 32 \text{ MN/m}^2$ rests on a relatively soft, elastically isotropic half-space with a modulus of elasticity of $E_u = 4 \text{ MN/m}^2$. In the second diagram, the shock wave already reaches the layer boundary. The difference in the propagation speeds in the two materials is clearly visible from the discontinuity in the iso lines where the layers meet. In the third diagram, the peak load ($\sigma_0 = 100\% \sigma_{0max}$) has already occurred and unloading has commenced. While this unloading is taking place, one can see how the shock wave progresses and deflections in the subsoil increase. While in Diagram 8, for example, deformation on the surface is already decreasing, it is still increasing at a depth of 1 m. The right half of the Table shows how the unloaded plate swings back. The footage from which these images were taken demonstrates what happens in this dynamic test and can be used for testing the plausibility of the results.

| | | |
|--|--|--|
| dynamische Lastplatte z-Verschiebung $E_0 E_u = \frac{3000000}{\Delta z_{0.01m}} = 9_{11}$ | ly symmetric geometry, lay thickness t 30 | dynamische Lastplatte z-Verschiebung $E_0 E_u = \frac{3000000}{\Delta z_{0.01m}} = 9_{11}$ |
| dynamische Lastplatte z-Verschiebung $E_0 E_u = \frac{3000000}{\Delta z_{0.01m}} = 9_{11}$ | | dynamische Lastplatte z-Verschiebung $E_0 E_u = \frac{3000000}{\Delta z_{0.01m}} = 9_{11}$ |
| dynamische Lastplatte z-Verschiebung $E_0 E_u = \frac{3000000}{\Delta z_{0.01m}} = 9_{11}$ | | dynamische Lastplatte z-Verschiebung $E_0 E_u = \frac{3000000}{\Delta z_{0.01m}} = 9_{11}$ |
| dynamische Lastplatte z-Verschiebung $E_0 E_u = \frac{3000000}{\Delta z_{0.01m}} = 9_{11}$ | | dynamische Lastplatte z-Verschiebung $E_0 E_u = \frac{3000000}{\Delta z_{0.01m}} = 9_{11}$ |
| dynamische Lastplatte z-Verschiebung $E_0 E_u = \frac{3000000}{\Delta z_{0.01m}} = 9_{11}$ | | dynamische Lastplatte z-Verschiebung $E_0 E_u = \frac{3000000}{\Delta z_{0.01m}} = 9_{11}$ |

3.3. The measuring depth of the dynamic load plate – results of the BEM simulation versus experimental investigations

The measuring depth of a test method is defined as the depth below which changes in the subsoil behaviour have no material influence on the results of the test.

Figure 9 shows an experimental investigation of the measuring depth of the dynamic load plate [2], [11].

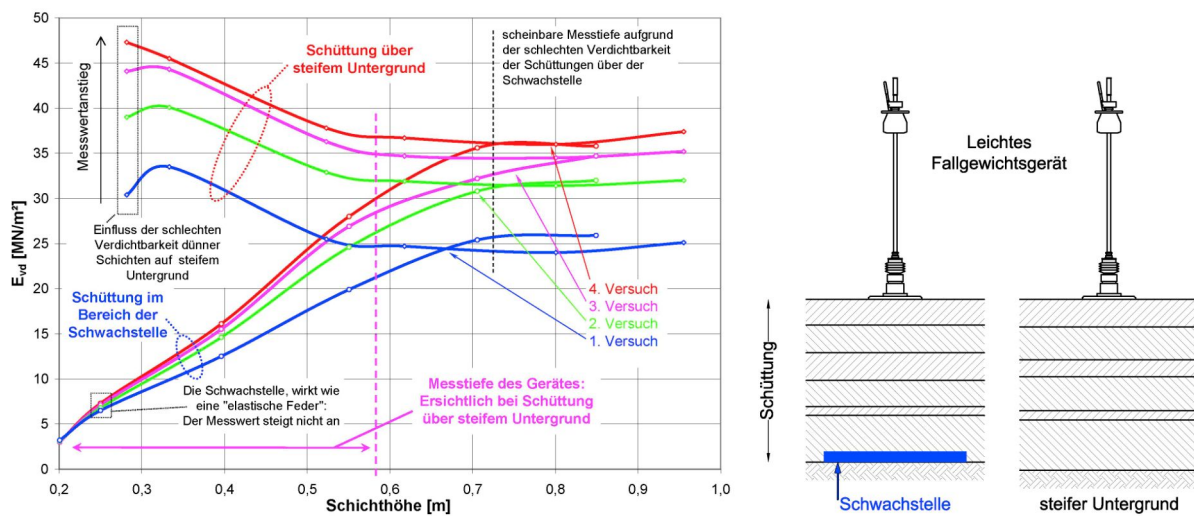


Fig. 9: Testing for weak spots: Experimental determination of the measuring depth of the dynamic load plate by covering a weak spot by layers of material

For the experimental determination of the measuring depth, an artificial weak spot was created by placing a mattress onto stiff ground and then covering it with extensive layers of material. Each layer of material was compacted by means of dynamic rollers and finally tests were carried out with the dynamic load plate. Each of the tests consisted of three pulses. Each deflection was measured, mean value was calculated and from this the modulus was derived according to equation (2). As the tests took place at one single point and the plate was not moved between the tests, each new test produced a higher value, which can be explained by the soil compaction taking place in the course of the test. Where only a small quantity of material was placed above the weak spot, the latter's influence is still substantial but the compaction effect described is not yet identifiable as soil above such a weak spot is hardly susceptible to compaction (Fig. 9: bottom left). Above stiff soil, the values recorded are significantly higher and the compaction effect can be seen from the rise in the values

measured, each of which approaches a limit value (Fig. 9: top left). As the layer thickness increases, the influence of the subsoil and the weak spot declines and the respective lines converge. The level where they meet or turn horizontal marks the measuring depth of the dynamic load plate. It is interesting to note that above stiff ground the lines tend to become horizontal already from a layer depth of about 60 cm, which corresponds to the actual measuring depth of the dynamic load plate. Above the weak spot, by contrast, the values measured converge much more slowly, misleadingly indicating a measuring depth of about 75 cm. This can be explained by the fact that the soil immediately above the weak spot can hardly be compacted for lack of counter-pressure. Thus, from a layer depth of about 60 cm of fill material, the dynamic load plate records not the weak spot but the poorly compacted area above it.

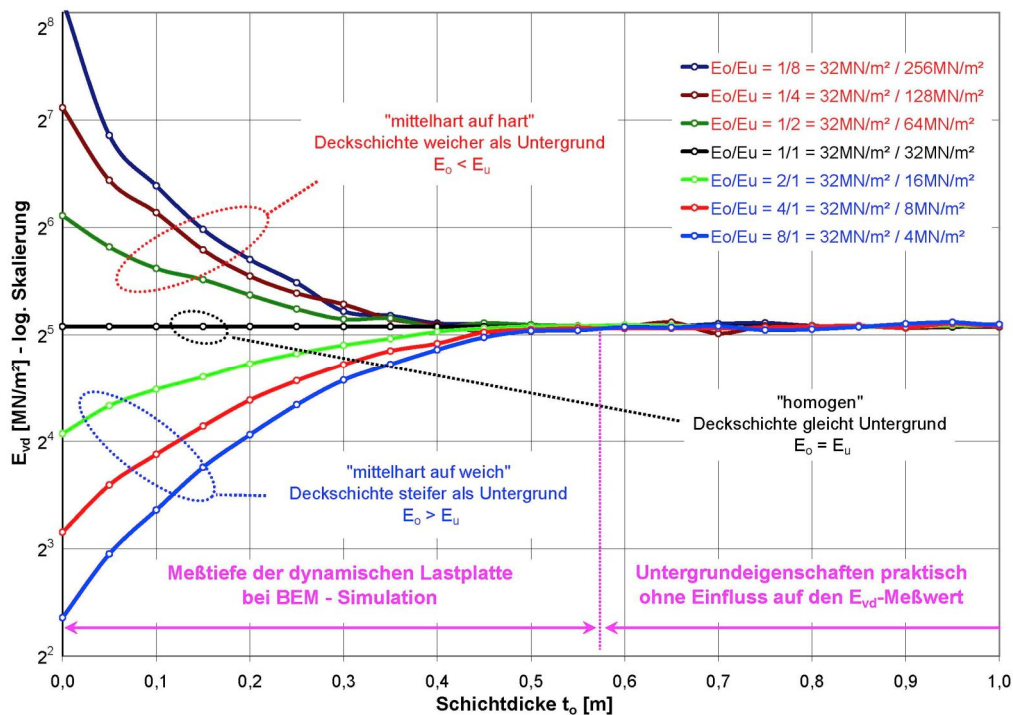


Fig. 10: Dynamic deformation modulus E_{vd} [MN/m²] on a two-layer subsoil with varying layer thickness t_o in semi-logarithmic representation. Simulation by means of the substructure method using BEM (transmission functions without material damping). Dynamic load plate ($r = 150$ mm, $m = 20$ kg) mit $E_o = 32$ MN/m², $\nu = 0.212$ [7].

The result of parameter studies done by means of BEM simulation is shown in Figure 10. For the cover layer with variable layer thickness t_o a modulus of elasticity of $E_o = 32$ MN/m² was assumed, whereas the modulus of elasticity of the subsoil E_u was set at 4, 8, 16, 32, 64, 128 and 256 MN/m² (2^2 , 2^3 , 2^4 , 2^5 , 2^6 , 2^7 , 2^8). The ratio of the modulus of elasticity E_o/E_u thus varies from 8/1 (“medium-hard on soft”) and 1/8 (“medium hard on hard”). Figure 10 shows the deformation modulus E_{vd} computed from the deformations by means of Equation 2 against

the thickness of the cover layer t_o and different moduli of elasticity. On the left of the diagram, the thickness of the cover layer is zero; therefore, the deformation modulus corresponds to the solution for the homogenous half-space with the material properties of the subsoil (E_u). Especially where the level of E_{vd} is low, the dynamic deformation modulus is higher than the corresponding static deformation modulus, as, among other things, larger displacements also activate inertial forces that under the brief loading of the test misleadingly point to a higher system stiffness. The further one pursues the lines in the diagram to the right, the thicker the cover layer becomes, causing the influence of the cover layer material (E_o) to rise while the influence of the subsoil (E_u) declines. Therefore, as the thickness of the layer increases, the lines converge towards the black line, which represents the solution of the homogeneous half-space with cover layer properties. The measuring depth has been reached when the subsoil properties no longer have any appreciable influence on the result and the lines in the diagram have thus reached the black line. In Figure 10, this is the case at a layer thickness of about 0.60 m, which is quite consistent with the experimental results.

4. CONCLUSION

The boundary element method is ideally suited for the computation of linear-elastic problems. As the BEM program used allowed only a very limited number of possible time steps in dynamic calculations, it was not possible to carry these out in the time domain. Therefore, the substructure method had to be used in the numerical simulation of the dynamic plate load test. The boundary element method was used only for determining transmission functions (in the frequency domain) of a substructure of the mechanical simulation model, while the solution for the second substructure and the coupling of the two structures had to be obtained by means of different programs. Automation of the variation of geometric conditions (layer thickness) and material parameters allowed the performance of extensive parameter studies which, for example, were required for the numerical investigations of the measuring depth of the dynamic load plate. The results of the numerical studies were also analysed graphically and provided plausible results, as is demonstrated by the good consistency of the experimentally and the numerically determined measuring depth of the dynamic load plate.

LITERATURE

- [1] Adam, D., Kopf, F., Adam, C. (2003): *Der dynamische Lastplattenversuch mit dem Leichten Fallgewichtsgerät – Theoretische und experimentelle Untersuchungen*. Bauingenieur, Band 79, Springer VDI Verlag, Düsseldorf.
- [2] Banerjee, P.K (1994): *The boundary element methods in engineering*. McGraw-Hill, London.
- [3] Brandl, H., Adam, D., Kopf, F., Niederbrucker, R. (2003): *Der dynamische Lastplattenversuch mit dem Leichten Fallgewichtsgerät*. Bundesministerium für Verkehr, Innovation und Technologie, Straßenforschung, Heft 528, Wien
- [4] Heuer, R. (2001/02): *Randelementmethoden*. Studienblätter zur gleichnamigen Lehrveranstaltung. Institut für Allgemeine Mechanik, Technische Universität Wien.
- [5] Kopf, F., Adam, D. (2003): *Der dynamische Lastplattenversuch mit dem Leichten Fallgewichtsgerät*. Tagungsband 4. Österreichische Geotechniktagung, ÖIAV, Wien
- [6] Mähr, T. (2002): *Anwendung der Randelementmethode in der Geotechnik unter Verwendung des Computerprogrammes GPBEST*. Großer Entwurf. Institut für Grundbau und Bodenmechanik, Technische Universität Wien.
- [7] Paulmichl, I. (2004): *Numerische Simulation von statischen und dynamischen Verdichtungskontrollen auf geschichteten Halbräumen mit der Randelementmethode*. Diplomarbeit. Institut für Grundbau und Bodenmechanik, Technische Universität Wien.
- [8] Pivonka, P. (1996): *Lösung von ebenen Elastizitätsproblemen mit Hilfe der Randelementmethode unter Verwendung des Computerprogrammes GPBEST*. Diplomarbeit. Institut für Allgemeine Mechanik, Technische Universität Wien.
- [9] Schwab, E., Szabo, S., Tykal, J. (1991): *Tragfähigkeits- und Dichteüberprüfung mittels dynamischer Lastplatte*. Bundesministerium für wirtschaftliche Angelegenheiten. Straßenforschung, Heft 394, Wien.
- [10] Technische Prüfvorschriften für Boden und Fels im Straßenbau TP BF – StB, Teil B 8.3 (2003): *Dynamischer Plattendruckversuch mit Leichtem Fallgewichtsgerätes*. Forschungsgesellschaft für Straßen- und Verkehrswesen, Arbeitsgruppe Erd- und Grundbau.
- [11] Vergeiner, R. (1999): *Experimentelle Untersuchungen zur dynamischen Lastplatte*. Diplomarbeit. Institut für Grundbau und Bodenmechanik, Technische Universität Wien.

- [12] Weingart, W. (1977): *Theoretische und experimentelle Untersuchungen zur Bestimmung der Elastizität, Viskosität und Festigkeit von Erdstabilisierungen mit Hilfe einer registrierenden Kleinschlagsonde*. Dissertation. Technische Hochschule Leipzig.
- [13] Weingart, W. (2001): *Bestimmung dynamischer Tragfähigkeitskennwerte mit Hilfe von Fallgewichtsgeräten bei Labor- und Feldversuchen*. Tagungsband 1. Siegener Symposium: Messtechnik im Erd- und Grundbau, Universität Siegen.